Atmospheric Pollution Research 16 (2025) 102367

Contents lists available at ScienceDirect

Atmospheric Pollution Research

journal homepage: www.elsevier.com/locate/apr

Characterization of equivalent Black Carbon (eBC) in different environments in the western Mediterranean

Violeta Matos [a,*], Víctor Estellés [a], Josep Camarasa [a], Mar Sorribas [b], María Pilar Utrillas [a]

[a] Solar Radiation Research Group, Department of Earth Physics and Thermodynamics, Universitat de València, Carrer Doctor Moliner, 50, Burjassot, 46100, Valencia, Spain

[b] Atmospheric Sounding Station – El Arenosillo, Atmospheric Research and Instrumentation Branch, INTA, Crta. San Juan del Puerto- Matalascañas, km 34, Mazagón, 21130, Huelva, Spain

ARTICLE INFO

Keywords:
Equivalent Black Carbon
Mann–Kendall test
Urban pollution
Rural background pollution

ABSTRACT

This work is focused on the characterization of equivalent Black Carbon (eBC) mass concentrations at two sites (suburban and rural background) in Valencia, Spain. The suburban station is in the metropolitan area of Valencia (the third largest in Spain), so the analysis of eBC is crucial to determine its impact on urban pollution. The mean (±standard deviation) concentration from April 2011 to March 2023 was 1.0 ± 0.5 μgm^{-3}, ranging from 0.7 μgm^{-3} in summer to 1.4 μgm^{-3} in winter. The seasonality is related to the intraannual variability of the Boundary Layer Height (BLH) and the daily variation is closely related to the daily traffic pattern, especially to rush hours. Applying the Mann–Kendall test, eBC levels exhibited decreasing trends for all seasons, showing slopes between −15%/yr and −5%/yr. In addition, the Absorption Ångström Exponent shows a significant upward trend for all periods analyzed.

The rural station is in a remote site at 1280 m.a.s.l., 80 km from the suburban station. The overall mean from 2017 to 2023 (± standard deviation) was 0.17 ± 0.14 μgm^{-3}, ranging from 0.08 μgm^{-3} in winter to 0.20 μgm^{-3} in summer. This seasonality is due to a combined effect of local dynamics of the BLH and the station altitude. The daily variability is smoother, without marked changes. The maximum daily concentration is reached in the late afternoon. According to the Conditional Bivariate Probability Function (CBPF) diagrams, the transport from the city of Valencia (SE direction) is the most relevant contribution at the measurement location.

1. Introduction

The growing concern about the health and environmental effects of unregulated air pollutants, known as *air pollutants of emerging concern*, has resulted in the future inclusion of some of them (ultrafine particles, black carbon, ammonia) in the European Union Ambient Air Quality Directives (AAQD), in order to align EU air standards more closely with World Health Organization (WHO) recommendations (Council of the European Union, 2023). The proposal highlights the importance of monitoring the pollutants of emerging concern, in order to support scientific understanding of their effects on health and the climate. The proposal also requires a minimum number of sampling points for fixed measurements (*supersites*) at urban background and rural background locations.

The adverse health effects related to air pollutants inhalation have been studied in recent years due to a growing concern about air quality related to urban development, industrialization, etc (WHO, 2021; EEA, 2022). WHO estimates that around 6.7 million deaths, mainly from noncommunicable diseases, are related to the combined effects of ambient air pollution and household air pollution. Many studies have shown the relation between high concentrations of Particulate Matter (PM) and respiratory diseases (Bernstein et al., 2004), lung cancer (Shivani et al., 2019) and the increase of the risk of cognitive impairment and dementia (Peters et al., 2019).

The effects of aerosols on climate can be direct or indirect. Directly, aerosols absorb and scatter solar radiation; indirectly, they have influence on cloud formation by acting as condensation nuclei, also affecting the lifetime of clouds and their reflectivity (Lohmann and Feichter, 2005). Radiative Forcing (RF) is the metric used to quantify the influence of external factors on the Earth's climate and energy balance. The total RF of aerosols has two competing components: the dominant cooling effect due to aerosol scattering and a certain warming compensation due to the absorption of solar radiation by some absorbing aerosols.

* Corresponding author.
E-mail address: violeta.matos@uv.es (V. Matos).

https://doi.org/10.1016/j.apr.2024.102367
Received 5 July 2024; Received in revised form 18 November 2024; Accepted 19 November 2024
Available online 26 November 2024

The carbonaceous aerosols are one of the most relevant fraction of atmospheric PM, generally ranging between 20% and 50% of the total aerosol mass (Kanakidou et al., 2005; Putaud et al., 2010). The carbonaceous fraction includes an organic fraction, known as organic aerosols (whose absorbing component is Brown Carbon, BrC) and a refractory and absorbing component known as *Elemental Carbon* (EC, quantified using thermo-optical methods) or *equivalent Black Carbon* (eBC, determined by optical methods) (Petzold et al., 2013).

BC is one of the most relevant carbonaceous of fine particulate air pollution ($PM_{2.5}$) and a short-lived climate forcer. BC is mainly characterized by its strong absorption capacity of solar radiation and its resistance to chemical transformations (Bond et al., 2013). In addition, BC is related to formation and modification of cloud properties processes (Lohmann and Feichter, 2005; Spracklen et al., 2011; Sand et al., 2020), the perturbation of the atmospheric temperature profile (Koch and Del Genio, 2010; Ding et al., 2016; Hu et al., 2022) and the altered melting of snow and ice sheets, affecting the terrestrial albedo (Ji, 2016; Lee et al., 2017; Kang et al., 2020). In addition to effects on the climate system, BC is also associated with health effects (Janssen et al., 2011), mainly related to increases in premature mortality from cardiovascular and respiratory diseases and lung cancer (Beelen et al., 2008; Li et al., 2016; Ljungman et al., 2019; Farzad et al., 2020), but also with effects on the brain and cognitive impairment (Freire et al., 2010; Power et al., 2011).

Observed changes in climate are unequivocal at the global scale and increasingly apparent on regional and local spatial scales. Information from a variety of sources (global but also regional and local) is particularly relevant in the context of co-producing regional-scale climate information to support decision-making. The latest IPCC (Intergovernmental Panel on Climate Change) report (IPCC, 2021) emphasizes the relevance of observations on regional and local scales especially for two reasons: to enable the evaluation of the environmental repercussions of policy decisions and to understand how much of observed recent climate change can be attributed to anthropogenic forces or natural variability. Furthermore, regional information from multiples lines of evidence can vary substantially from one case to other. New local monitoring stations (especially in urban areas) provide key information to enhance the understanding of microclimates and improve parameterizations.

This work describes the temporal variations of eBC mass concentrations in two representative sites of suburban (12 years) and rural background (6 years) conditions in Valencia (western Mediterranean sea). The temporal variations include different time scales: interannual, intraannual, seasonal and daily. Atmospheric variables and traffic intensity are also analyzed in this study. Complementary, the temporal trends of eBC concentrations over the last 12 years are studied by applying the Mann–Kendall and Sen's slope estimator non-parametric test. This test allows to determine the existence (or not) of an increasing or decreasing trend over time, including the annual rate of change.

2. Measurement site description

2.1. Suburban and rural measurement stations

The suburban station is the Atmospheric Pollution Laboratory (LCA, Laboratorio de Contaminación Ambiental), which is part of the Burjassot AtmoSpheric Station (BASS), located in the Burjassot Campus of the University of Valencia (39.507° N, 0.420° W, 60 m.a.s.l.).

Burjassot is situated in the metropolitan area of Valencia, in the eastern coast of Spain and it has a population of 39,702 inhabitants. Valencia has one of the largest metropolitan areas in the country, where the total population is 1,599,656 inhabitants, from which 807,693 live in Valencia city. Burjassot is located 5 km northwest from Valencia city center and its distance to the western coast of the Mediterranean Sea is about 10 km (Fig. 1).

The BASS is located in the proximity to a six-lane highway (CV-35), being one of the main roads leading to the center of Valencia, and its traffic intensity is high (> 100k vehicles/day) especially during rush hours (~ 14k vehicles at 7–8 LT). The traffic intensity (expressed in number vehicles per hour) is monitored by the local authorities, for both ascending and descending directions (Fig. 1), and has a strong influence on the local aerosol type (Matos et al., 2020). The BASS is occasionally affected by particles brought from the Sahara Desert, industrial continental Europe or maritime and oceanic source regions (Esteve et al., 2012a). In addition, the site is commonly affected by seasonal agricultural activities (such as burning of biomass debris, or resuspension of particles by soil preparation) (Estellés et al., 2005) and forest fires (mainly in summer) (Gómez-Amo et al., 2017). Due to the location and anthropogenic influences, the BASS is considered to be a suburban traffic station.

The rural background measurement station is located at the Astronomical Observatory of the University of Valencia (OAO, Observatorio astronómico de Aras de los Olmos) (39.945° N 1.102° W, 1380 m.a.s.l.), in the municipality of Aras de los Olmos. The measurement site is located on the Muela de Santa Catalina, about 80 km from the city of Valencia in a northwesterly direction, while Aras de los Olmos is 3.5 km away. Due to the difference in altitude, agricultural burning is expected to have low influence on the measurements. Another possible source of aerosols could be wood burning in winter. The population of the municipality is 380 inhabitants. For all this, and due to its geographical location, the station has a continental climate with very low levels of atmospheric pollution.

2.2. Instrumentation

The main instrumentation consists of two optical filter instruments for measuring the absorption coefficient (b_{abs}), from which the eBC mass concentrations are derived.

The aethalometer is one of the most widely used instruments for real-time measurement of absorption properties of atmospheric particles (Weingartner et al., 2003; Hansen, 2005). From April 2011 to March 2023, an Aethalometer model AE31 (Magee Scientific) has been installed and operated at the suburban station in order to obtain the b_{abs} from light attenuation measured at seven wavelengths covering the UV (370 nm), VIS (470, 520, 590, 660 nm) and NIR (880, 950 nm). The AE31 is a filter-based instrument and its measuring principle is based on the determination of the attenuation measured by two photodetectors (one as a reference) while the filter continuously collects the aerosol samples. The eBC accumulation rate in the filter is proportional to the eBC concentration in the air sample and the air flow rate. From the raw measurements of the two photodetectors, the attenuation of the beam (ATN) at a given time and for each wavelength can be obtained:

$$ATN(\lambda,t) = -100 \ln\left(\frac{I(\lambda,t)}{I_0(\lambda,t)}\right) \tag{1}$$

where the factor 100 is for numerical convenience (Hansen, 2005). I_0 is defined as the intensity of light transmitted through the original filter (reference), being I the intensity of light transmitted through the portion of the filter on which the aerosols are collected. The attenuation coefficient, b_{atn}, is obtained from the change in attenuation that the beam suffers through the filter during a time interval Δt:

$$b_{atn} = \left(\frac{ATN(\lambda, t+\Delta t) - ATN(\lambda,t)}{\Delta t}\right)\cdot\frac{A}{V} \tag{2}$$

where A is the spot area (1.67 cm^2) and V is the flow rate (4 L min^{-1}). b_{atn} differs from the b_{abs}, due to three systematic effects on the measurements: *loading*, *multiscattering* and *single scattering*. The compensation of these effects is based on different algorithms proposed in the literature: Weingartner et al. (2003), Arnott et al. (2005), Schmid et al. (2006), Virkkula et al. (2007) and Collaud Coen et al. (2010), although reference values that have been obtained in other works are usually used due to the inability to determine them experimentally (Sciare

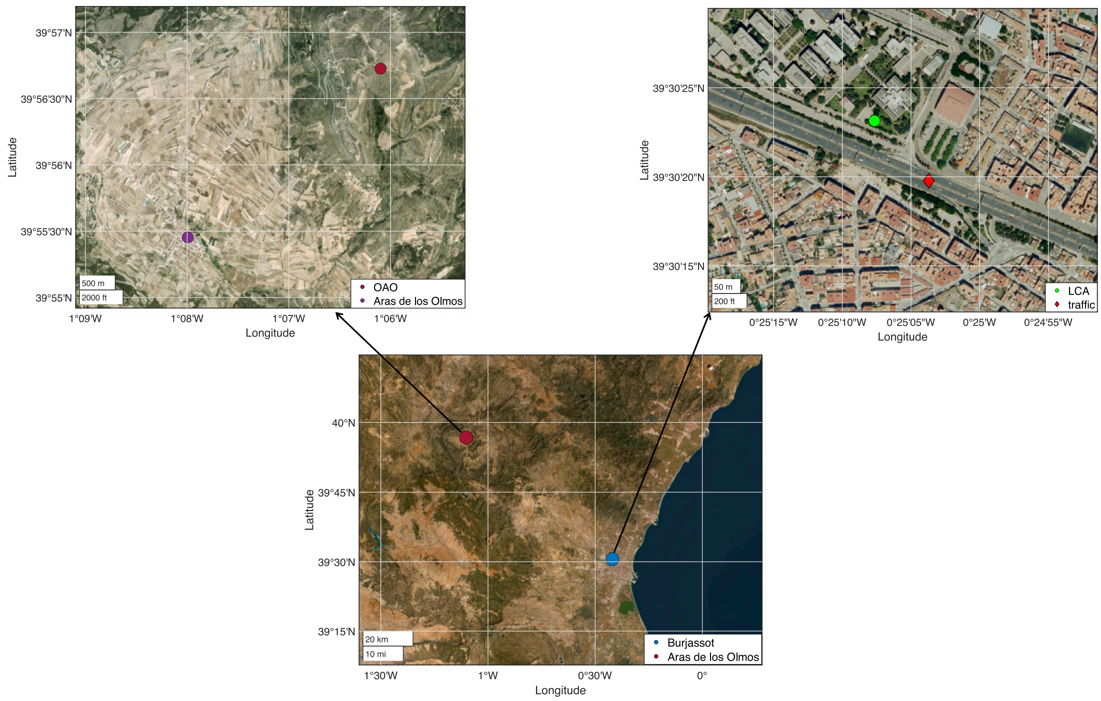

Fig. 1. Location of the measurement sites: suburban station (LCA) and rural background station (OAO).

et al., 2011; Müller et al., 2011; Zanatta et al., 2016; Wang et al., 2018). Due to the seasonal variations of the aerosol optical and radiative properties at the BASS location, which have been previously analyzed by Estellés et al. (2007), Esteve et al. (2012b) and Segura et al. (2016), the AE31 measurements requires a specific-site compensation. In this work, the compensation proposed by Segura et al. (2014) and applied for our site in Segura et al. (2016) is used, because the procedure is completely experimental. This experimental compensation allows us to obtain the spectral dependence of the parameters.

A Multi-Angle Absorption Photometer (MAAP) model 5012 (Thermo Scientific) has been used for monitoring rural background eBC concentrations in Aras de los Olmos. This instrument measures the light transmitted and backscattered by a particle-loaded filter at 637 nm (Müller et al., 2011), operating at a constant flow rate of 16.7 L min^{-1}. During the period February 2013–February 2015, it was installed at the BASS site to analyze the consistency with the aethalometer measurements and obtain the compensation factors for the AE31 (Segura et al., 2016).

The principle of measuring of the MAAP is the same as that of the aethalometer, being well documented during the instrument development (Petzold and Schönlinner, 2004). The key principle of the MAAP is that it has three photodetectors whose position allows the measurement of the signal transmitted (0°) but also scattered by the aerosols (130°, 165°). Because of that, the scattering effects are compensated internally by the instrument, without the need to calculate external compensation parameters. Additionally, by applying a radiative transfer scheme for the particle-loaded filter, the aerosol-filter layer alone and the black filter alone, the single scattering albedo and the optical depth of the aerosol loaded filter are calculated to estimate the b_{abs}. The eBC concentrations are derived from b_{abs} using a manufacturer's standard value of scattering cross-section: σ_{BC} = 6.6 m^2g^{-1}.

2.3. Atmospheric data

In addition to traffic intensity, the atmospheric variables were used in this work to understand the temporal variations observed in the eBC concentrations. Meteorological variables (temperature, relative humidity, wind speed, pressure and precipitations) were monitored at both locations with two Vaisala Weather Transmitter WXT520 sensors.

To explain the patterns (daily and seasonal) of the atmospheric properties and aerosol concentrations, it is also necessary to understand the changes of the Atmospheric Boundary Layer (ABL). In this work, ERA5 data reanalysis from ECMWF (European Centre for Medium-Range Weather Forecasts) (Hersbach et al., 2020) meteorological global model was used to obtain hourly data of the Boundary Layer Height (BLH), with a spatial resolution of 0.25° ×0.25° (latitude × longitude) and 1 h of temporal resolution.

3. Methodology

3.1. Compensation of the AE31 measurement

Basically, there are two empirical factors that have to be calculated to infer the b_{abs} from the b_{atn} from AE31 (Eq. (2)): C (describing the enhancement of absorption by particles in the filter matrix due to multiple scattering of light) and f (compensating the loading effect). The b_{abs} can be obtained using the following expression:

$$b_{abs}(\lambda) = \frac{b_{atn}(\lambda)}{C \cdot \left[\left(\frac{1}{f(\lambda)} - 1\right) \cdot \frac{ln(ATN(\lambda)) - ln(10\%)}{ln(50\%) - ln(10\%)} + 1\right]} \quad (3)$$

being f the *shadowing factor*. This parameter was calculated by minimizing the difference between the ratio of b_{abs} before and after the filter portion change (Sandradewi et al., 2008; Segura et al., 2014). The median f values are plotted as a function of λ and fitted with a linear equation. Values obtained for these parameters were recalculated using the AE31 measurements until March 2023. The f values present slight seasonal variations, as well as spectral dependence.

To calculate the C parameter in Eq. (3), Segura et al. (2014) proposal combines the compensation of Weingartner et al. (2003) and Schmid et al. (2006). First, the b_{atn} from the AE31 are compared with a reference instrument: the MAAP. To obtain the spectral dependence of C, the parameterization proposed by Schmid et al. (2006) (based on Arnott et al. (2005)) was applied. This method requires complementary instrumentation to measure reference absorption and scattering coefficients (b_{scat}). The MAAP was installed in BASS from 2013 to 2015, when it was moved to another rural station, for monitoring regional background pollution. Therefore, the spectral parameters

C_λ were obtained from these two measurement years. The procedure is explained in detail in Segura et al. (2014, 2016). The site-specific C-values obtained by Segura et al. (2016) were used in this work. Both parameters applied for experimental compensation in this study are shown in Table S1.

3.2. Conversion of $b_{abs}(\lambda)$ to eBC concentration

The process to obtain the BC concentration from optical methods is to derive it from the b_{abs} measurements. The Mass Absorption Cross section (MAC) is essential for the determination of the eBC concentration from the b_{abs}, so it is fundamental to identify the correct value for the conversion:

$$eBC(\lambda) = \frac{b_{abs,\lambda}}{MAC_\lambda} \tag{4}$$

There are multiples variables with influence on MAC such as particle size, morphology or mixing state (Fuller et al., 1999; Schnaiter et al., 2005; Bond et al., 2006; Zanatta et al., 2016; Zotter et al., 2017; Zhao et al., 2021), as well as location or measurement limitations (Bond and Bergstrom, 2006). Due to the lack of instrumentation needed to determine the MAC experimentally, it is important to select a well-representative value for our station. In this work, a reference MAC value obtained at an urban background site in Barcelona (Spain) by Yus-Díez et al. (2022) was used, which is 7.55 ± 2.06 m^2g^{-1} at 950 nm. The main factor taken into account for the selection of this reference value is the strong traffic local influence at both locations, in addition to similar atmospheric conditions and geographical situation.

3.3. Mann–Kendall and Sen's slope estimator

The Mann–Kendall test (MK) (Mann, 1945; Kendall, 1975) and Sen's slope estimator (Theil, 1950; Sen, 1968) were used to determine the existence of temporal trends (increasing/decreasing) and the magnitude of the trend, respectively, of the concentrations of eBC. The MK test is a particularly useful non-parametric test for estimating aerosol properties trends, because it allows missing values in the database, negatives or values below the detection limits (Collaud Coen et al., 2013, 2020a). This method can be used because the MK test uses only the relative magnitude of the data rather than their measured values (Gilbert, 1987). In addition, the MK test does not require the data to be normally distributed.

The existence of a statistically significant trend is the consequence of rejecting the null hypothesis of randomness or no trend, H_0 (i.e. data $x_1, x_2, \ldots, x_n$ are a sample of n independent and identically distributed values), against the alternative hypothesis of a two-sided trend, H_1 (x_k and x_j are not identically distributed for all k, with $j \le n$ and $k \ne j$). The test statistic S is defined as:

$$S = \sum_{k=1}^{n-1} \sum_{j=k+1}^{n} sgn(x_j - x_k) \tag{5}$$

where

$$sgn(x_j - x_k) = \begin{cases} 1 & \text{if } x_j - x_k > 0 \\ 0 & \text{if } x_j - x_k = 0 \\ -1 & \text{if } x_j - x_k < 0, \end{cases} \tag{6}$$

When the number of values (n) in the time series is higher than 40, the normal approximation is used. Actually, Kendall (1975) showed that this approximation may be used for n as small as 10 unless there are many tied data (Gilbert, 1987). The standard normal variate Z is obtained as:

$$Z = \begin{cases} \frac{S-1}{[VAR(S)]^{1/2}} & \text{if S} > 0 \\ 0 & \text{if S} = 0 \\ \frac{S+1}{[VAR(S)]^{1/2}} & \text{if S} < 0 \end{cases} \tag{7}$$

where VAR[S] and E[S] are the variance and mean of S under H_0, respectively (Kendall, 1975):

$$E[S] = 0 \tag{8}$$

$$VAR[S] = \frac{1}{18}\left[n(n-1)(2n+5) - \sum_{p=1}^{g} t_p(t_p-1)(2t_p+5)\right] \tag{9}$$

being g the number of tied groups and t_p the number of data in the pth group.

Finally, in a two-sided test for trend, the H_0 should be accepted if $\|Z\| \ge z_{1-\alpha/2}$ where $F_N(z_{1-\alpha/2}) = \alpha/2$, F_N being the standard normal cumulative distribution function, where α is the significance level for the test (Gilbert, 1987; Hirsch et al., 1982).

When data show seasonal cycles, they should be taken into account before applying the MK test. Hirsch et al. (1982) extended the MK test to account for seasonality, which is known as the seasonal MK test. Basically, daily medians concentrations are segmented by meteorological seasons, and the Eqs. (5)–(9) are applied using the seasonal or monthly medians, instead of the annual ones.

Sen's slope estimator is closely related to the MK test, since it represents the magnitude of change. The Sen's slope represents the global slope of the entire time series, and it is calculated as the median of the N slopes between each pair of time values:

$$Q = \frac{x_{i'} - x_i}{i' - i} \tag{10}$$

where $x_{i'}$ and x_i are data values during time periods i' and i, respectively, and where $i' > i$. N is the number of data pairs where $i' > i$. The Sen's estimator of slope is the median of these N values of Q. The confidence limits (CL) of the slope may be obtained by a simple procedure proposed by Gilbert (1987) at a desired confidence level (α).

The MK test requires serially uncorrelated time series. Most of the aerosol properties and atmospheric processes often exhibit positive autocorrelation (Collaud Coen et al., 2020b). Positive autocorrelation usually leads to an erroneous increase in rejection of the null hypothesis of no trend, i.e. false positives (von Storch, 1999; Collaud Coen et al., 2020b). There are several methods proposed to eliminate or reduce the autocorrelation or ak_1, known as "prewhitening". Yue et al. (2002) proposed the *Trend-Free PreWhitening* (TFPW) procedure, compared by Collaud Coen et al. (2020b) with five other prewhitening algorithms, being one of the most common.

The daily medians of the eBC concentrations show a statistically significant autocorrelation, so the algorithm proposed by Yue et al. (2002) was applied before applying the seasonal MK test. Confidence levels of 80%, 90%, 95% and 99% were chosen to determine the existence of upward and downward statistically significant trends in the eBC concentrations. The annual trends are considered only if the seasonal slopes are homogeneous at the 90% confidence level.

3.4. CBPF diagrams

The directional and wind speed dependence of the concentrations were analyzed using a source identification method known as Conditional Bivariate Probability Function (CBPF), the bivariate extension of the commonly used Conditional Probability Function (CPF) (Uria-Tellaetxe and Carslaw, 2014). CBPF analysis provides a technique for identifying the directions and wind speeds associated with high concentration values, calculating the probability that in a particular wind sector, the concentrations of a pollutant are higher than a threshold. In our case, the threshold was set to the 75th percentile. This analysis was carried out utilizing the Openair R package (Carslaw and Ropkins, 2012; Carslaw, 2018).

4. Results and discussion

4.1. General statistics for both measurement sites

Tables S2 and S3 show the most relevant statistical values (mean, median, standard deviation, standard error, 10th percentile and 90th percentile) of the eBC concentrations in Burjassot and Aras de los Olmos, respectively. The statistics in Table S2 were calculated removing the confinement period (March 15–June 22, 2020). This period is separately analyzed in Section 4.2.1.

The concentrations in Burjassot are much higher than Aras de los Olmos levels, with means (± standard deviation) for the entire measurement period of 1.0 ± 0.5 μgm^{-3} and 0.17 ± 0.14 μgm^{-3}, respectively. The annual averages in Burjassot range between 0.8 and 1.2 μgm^{-3}, slightly higher than the annual medians, which are between 0.7 and 1.1 μgm^{-3}. The standard deviations show the high yearly variability of concentrations. The lowest values, represented by the 10th percentile, are between 0.34 and 0.55 μgm^{-3}, while the highest (90th percentile) are between 1.31 and 1.88 μgm^{-3}. The 90th percentile value in 2018 is the highest, but this is due to the instrument was only in operation for 117 days, corresponding to the months when concentrations are highest (winter). The average eBC levels at the Burjassot station are lower than those obtained in other urban areas of Spain, such as background urban stations in Granada (Casquero-Vera et al., 2021; Savadkoohi et al., 2023), Barcelona (Reche et al., 2011; Savadkoohi et al., 2023) and Madrid (Becerril-Valle et al., 2017). Generally, concentrations are higher at points located a few meters from a road (Reche et al., 2011; Helin et al., 2018; Taheri et al., 2019). The average values obtained in this study are in the range reported in the Helsinki Metropolitan area by Helin et al. (2018) and Saarikoski et al. (2021), and in several places in Ontario by Healy et al. (2017), with a strong influence of road traffic. Note that 2018 is not representative for comparing annual values, as there is only 30% valid data due to technical problems. On the other hand, the year 2023 has only three months of data, so it is also not representative. Both these years should be taken into account only in the case of performing analysis from a seasonal point of view, considering the month of valid measurements. The data in Table S2 show a certain reduction in some statistics over the years, in particular the annual medians. Excluding 2018 and 2023, two periods can be distinguished: 2011–2015, in which medians above 0.9 μgm^{-3} are reached; and 2016–2022, in which all values are below 0.9 μgm^{-3}. This decreasing trend is also observed in the 10th and 90th percentiles. The reduction in the eBC concentration has been observed across Europe in recent years, especially in urban and suburban regions (Sun et al., 2020; Luoma et al., 2021; Savadkoohi et al., 2023).

The concentrations of eBC at Aras de los Olmos do not show important interannual changes, with averages (± standard deviation) ranging between 0.14 and 0.20 μgm^{-3} all years with a minimum of 60% temporal availability (2017–2020). These values show the low but not negligible contribution of BC to the total aerosol mass in rural regions. The shorter temporal period of measurements limits the identification of interannual patterns. However, a decreasing trend is observed in the values of the 90th percentile, varying from 0.37 μgm^{-3} to 0.27 μgm^{-3}. The levels of eBC are similar to the levels measured in some regional background sites across Europe, such as the Mediterranean locations Montseny (Spain) and Finokalia (Greece) and the Scandinavian site Aspvreten (Sweden) (Zanatta et al., 2016). The eBC levels at Aras de los Olmos station are higher than those reported in higher altitude measurements stations.

4.2. Annual and seasonal variability

The interannual variation of the daily concentrations of eBC at both measurement sites is shown in Fig. 2. The difference in magnitude between the concentrations at both sites, which was already seen in Tables S2 and S3, is the most apparent from the comparison. At the Burjassot site, the daily eBC concentrations generally range between 0.3 and 3 μgm^{-3}, while in Aras de los Olmos the concentrations only occasionally exceed 0.4 μgm^{-3}. The highest eBC concentrations in Burjassot are observed in winter. In the case of Aras de los Olmos, the eBC concentration seems to reach higher values in the summer months. To facilitate the identification of seasonality, Box–Whiskers plots (based on daily data) are shown in Fig. 3 for both sites. The horizontal line in each box is the median (50th percentile), the edges of each box are the 25th and 75th percentiles, being the distance between the two extremes the interquartile range. The whiskers indicate the 5th and 95th percentiles. Data exceeding the whisker length are marked as outliers. The asterisk in each box is the mean value.

The monthly eBC concentrations in Burjassot (±standard deviation) vary from 1.4 ± 0.6 μgm^{-3} in December to 0.7 ± 0.3 μgm^{-3} in the summer months (June, July and August). The averages and medians of the monthly concentrations exceed 1 μgm^{-3} during winter and part of autumn, while in the central months of the year the concentration remains much lower (0.6–0.7 μgm^{-3}). In addition to this seasonality, the variability of the values is higher in the winter months (higher interquartile range). The seasonality of the eBC concentrations is mainly due to atmospheric conditions. Generally, severe pollution conditions in winter are related to a combined effect of lower BLH and frequent stagnant conditions (low wind speeds). The temporal characterization of the atmospheric variables (temperature, relative humidity, BLH, wind speed) is included in Figures S1 and S2. The seasonality of the eBC concentrations has a strong relation with BLH and wind speed seasonal patterns: more stable values and higher medians in summer, while in winter both variables show more variability and lower values.

In the case of Aras de los Olmos, the eBC concentrations show a completely opposite evolution: its highest values are reached in summer (~ 0.20 μgm^{-3}), and the lowest in winter (~ 0.08 μgm^{-3}), in addition to a greater variability of the values (higher interquartile range). In this case, the seasonality is also explained by attending to the local dynamics of the ABL. Figures S3 and S4 represent the interannual and intraanual evolutions, respectively, of atmospheric variables in Aras de los Olmos from 2017 to 2023, where it can be seen that the BLH reaches extreme annual values during winter. As in the case of Burjassot, the variability of the BLH observed in winter is higher, but in these months the means and medians of the BLH are lower, in many cases not exceeding 500 m. When the ambient temperatures are very low, especially during winter nighttime (Figure S3(a)) the convective motions of the air are more limited, causing the BLH to remain below the station and the ambient corresponds to the free troposphere conditions (Dumka et al., 2010); the measurements correspond to residual particles that remain above the ABL. Free troposphere conditions occur more frequently in winter than in summer, so this situation is common in high-altitude measurement stations (Motos et al., 2020; Sun et al., 2021). In the case of Aras de los Olmos the BLH reaches values above the 90th percentile (1566 m) more frequently in summer(~58%) than in winter (~6%); while in autumn and spring it reaches intermediate values (~15% and ~31%, respectively). In addition, the wind speed is more variable in winter than in summer (Figure S4(c)), which favors particle dispersion. The summer eBC concentrations in Aras de los Olmos are comparable to results reported by López-Caravaca et al. (2022) during one month (summer 2014) in Sierra de Aitana (Alicante, Spain), at 1558 m.a.s.l., being mean concentration (± standard deviation) 0.254 ±0.125 μgm^{-3}. At the same measurement station, Nicolás et al. (2018) also observed the same seasonality in PM concentrations.

4.2.1. Effects of lockdowns due to COVID-19

In March 2020, the Spanish government approved strict confinement measures to drastically reduce social, work and industrial activity to avoid the spread of the COVID-19 pandemic. The most strict lockdown lasted from March 14 to June 15, 2020. The effect that these measures had on the air quality in many countries was a significant decrease of the concentrations of major air pollutants, including

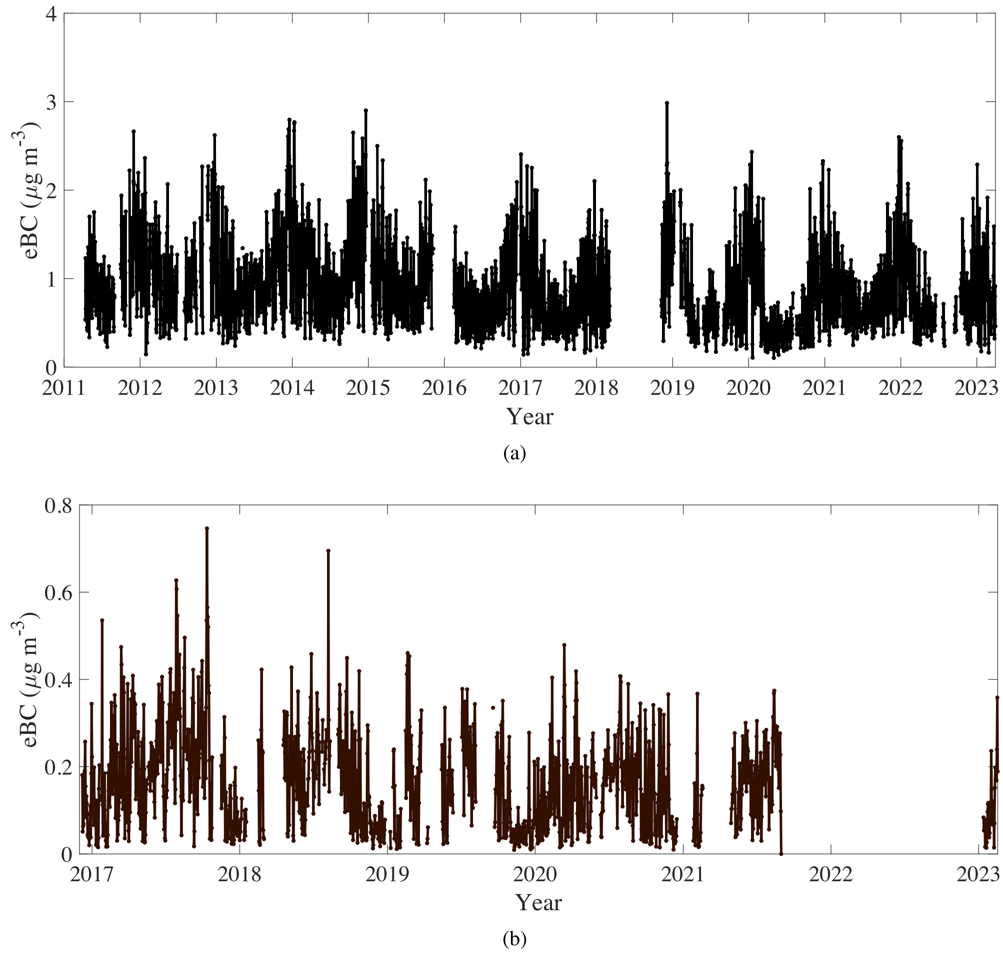

Fig. 2. Interannual evolution of daily mean concentrations of eBC at (a) Burjassot and (b) Aras de los Olmos sites.

BC (Evangeliou et al., 2021; Jia et al., 2021; Thomas et al., 2022; Rajesh and Ramachandran, 2022).

Compared to the same period before and after 2020 (2017–2019 and 2021–2023), daily traffic in the CV-35 highway was reduced by 60%. Figure S5 shows these decreases, corresponding to the confinement period (March 14–Jun 15), but also in February 2021, due to "perimeter closure" measures, which did not allow leaving the city of Valencia on weekends and during nighttime. Fig. 4(a) shows a Box–Whisker plot of the intraanual traffic pattern (based on daily traffic intensity) during 2020 and pre- and after-2020 (2017–2021 and 2021–2023). The most notable differences occur between March and June 2020, with higher variability in March and June. The reason was that the start of confinement measures was March 15 and the end on June 21, so traffic changed abruptly in the middle of the months. The monthly distribution indicates that for the rest of the year, the traffic remained slightly lower, following a similar annual pattern. Fig. 4(b) shows the Box–Whisker plot of the eBC levels in 2020 and during 2017–2023 excluding 2020. The decrease in traffic led to a shift in the annual pattern of the eBC concentrations at the measurement station, particularly during the months of confinement. Generally, the impact the traffic reduction has on the daily levels of eBC was a decrease between 40%–50% during March–June. Additionally, it should be noted that the daily concentrations in January and February of 2020 are slightly higher, approximately 20%, compared to the corresponding periods in other years. This variation is directly associated with the increased traffic intensity, as observed in Fig. 4(a). This phenomenon can be attributed to heightened concerns regarding the spread of COVID-19, following the initial health alerts issued by the WHO in December 2019. The observed rise in traffic may be due to a decline in the use of public transport and a corresponding increase in the use of private vehicles.

Table 1
Seasonal MK test statistics for eBC concentrations at the Burjassot station: number of seasonal data (N), test statistic (Z), Sen's slope (Sen), confidence intervals of the slope at the 90% confidence level (CI), interpretation of the trend (Trend): ↑ (increasing), ↓ (decreasing) and ⊗ (no trend); and significance level of the test (Sig.): $\alpha = 0.01$(****), 0.05(***), 0.1(**) and 0.2(*). DJF (December, January, February), MAM (March, April, May), JJA (June, July, August), SON (September, October, November).

	N	Z	Sen μgm^{-3}/yr (%/yr)	CI μgm^{-3}	Trend	Sig.
DJF	12	−1.44	−0.013 (−5.0)	(−0.025, −0.003)	↓	*
MAM	13	−2.99	−0.017 (−9.8)	(−0.024, −0.008)	↓	****
JJA	11	−3.74	−0.020 (−13.6)	(−0.025, −0.016)	↓	****
SON	12	−3.91	−0.032 (−15.0)	(−0.038, −0.029)	↓	****
Annual	48	−6.11	−0.022 (−11.0)	(−0.025, −0.018)	↓	****

4.2.2. *Annual and seasonal trends*

Decreasing trends of several aerosol optical and radiative properties have been observed in Europe (Collaud Coen et al., 2020a), especially in urban areas with intense traffic (Sun et al., 2020; Luoma et al., 2021; Savadkoohi et al., 2023), demonstrating the effectiveness of measures implemented in Europe to reduce anthropogenic emissions and to improve the air quality. This section is focused on analyzing the temporal trends of the eBC concentrations at the Burjassot site over the last 12 years. The seasonal MK test and Sen's slope estimator are used, and the slopes were normalized to facilitate the interpretation.

Fig. 5 and Table 1 show the seasonal Sen slopes and the statistics of the seasonal MK test the for the eBC concentrations, respectively.

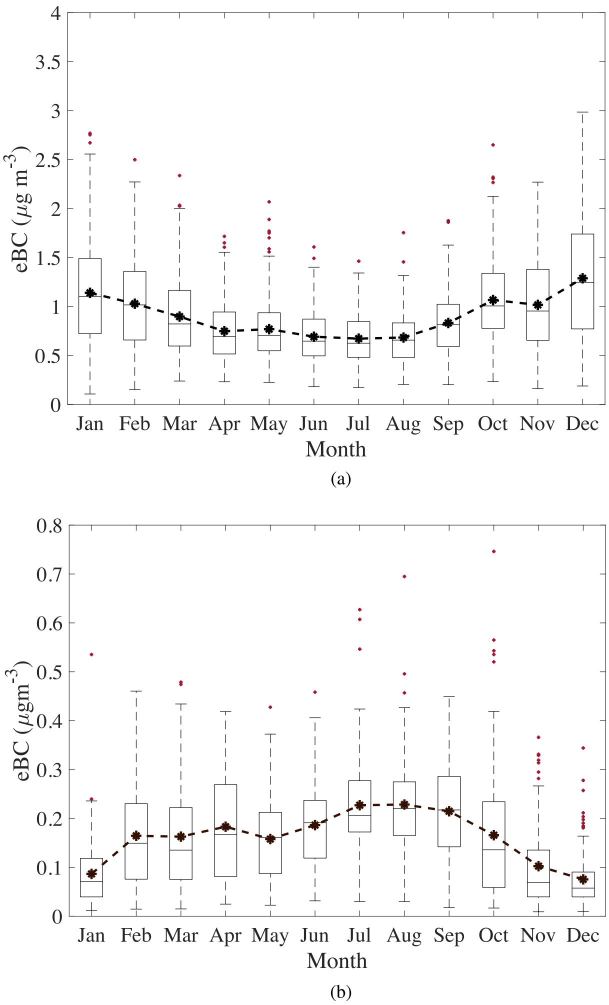

Fig. 3. Monthly Box–Whisker distribution (based on daily means) of eBC at (a) Burjassot and (b) Aras de los Olmos sites.

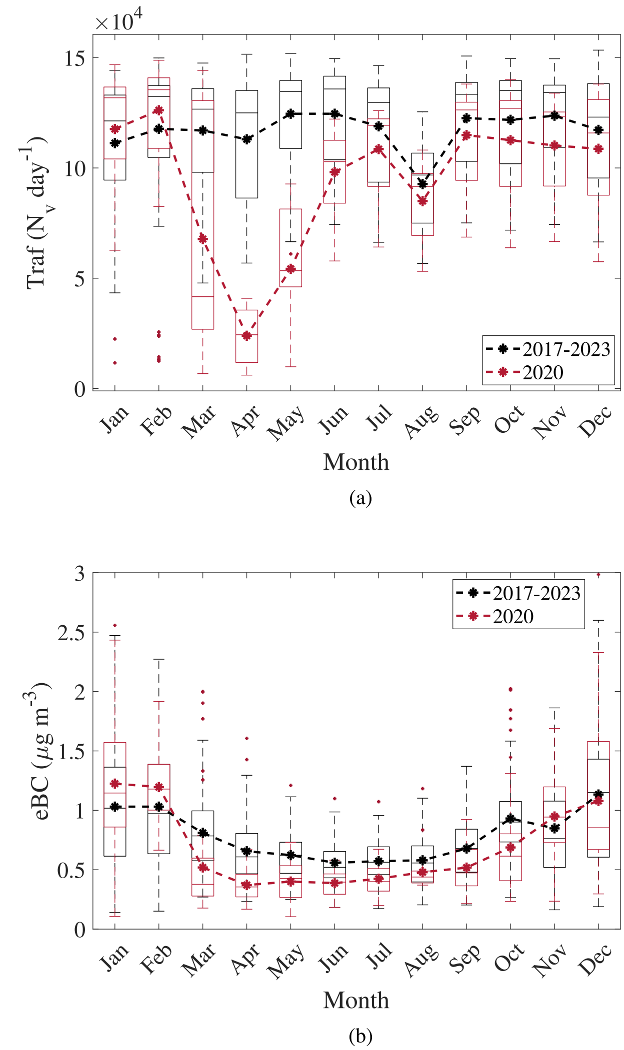

Fig. 4. Comparison of monthly box-whisker distribution (based on daily values) of (a) the traffic intensity and (b) the eBC concentrations in 2020 and 2017–2023 (excluding 2020).

Fig. 5 clearly illustrates that seasonal concentrations decrease annually, with a more moderate decrease in the winter levels. Statistically significant decreasing trends are observed in all seasons, with slopes from −15.0%/yr in autumn to −5.0%/yr in winter, at 99% and 80% confidence level, respectively. Except in winter, the seasonal eBC concentrations show statistically significant trends at the 99% confidence level. The interannual reduction of eBC is consistent with data reported in the NIAP (Spanish National Inventory of Atmospheric Pollutants): annual estimates of emissions of the main atmospheric pollutants, including NO_x, PM and BC are listed, corresponding to the period 1990–2021. Emissions of NO_x emitted by road transport in 2021 decreased by 50.7% since 1990 and 52.7% since 2011; while BC emission has been reduced yearly by percentages ranging from −7%/yr to −1%/yr. Compared to the 2011 data, the national BC emissions due to on-road traffic have decreased by 42%. These trends are similar to the results of Sun et al. (2020) at 16 stations in Germany, where the eBC concentration exhibited decreasing trends from 2009 to 2018 at the 95% confidence level. The trends exhibited by the eBC concentrations in Burjassot are also consistent with results reported by other works analyzing the temporal trends of eBC in urban areas, mainly in Europe.

To complement the temporal analysis of absorbing particles in our measurement site, the trends exhibited by the Absorption Ångström Exponent (AAE) were studied. This parameter was derived from the linear fit of the power-law representing the relationship between the

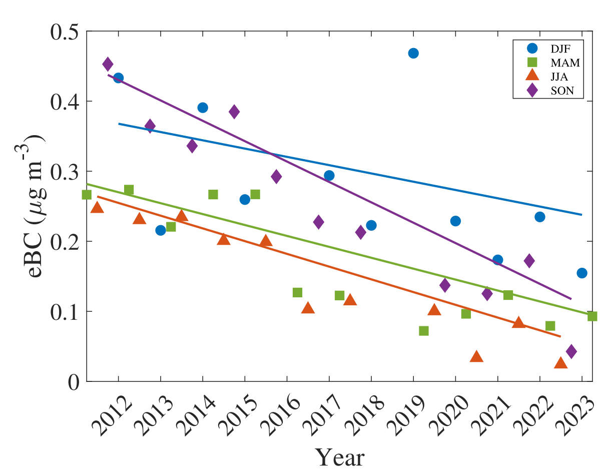

Fig. 5. Long-term trends exhibited by the seasonal eBC concentrations represented by Sen slopes (seasonal MK test) at the Burjassot site.

b_{abs} and the seven wavelengths measured by the Aethalometer. The statistics values of the seasonal MK test applied to the daily medians of

Table 2
Seasonal MK test statistics for AAE at the Burjassot station: number of seasonal data (N), test statistic (Z), Sen's slope (Sen), confidence intervals of the slope at the 90% confidence level (CI), interpretation of the trend (Trend): ↑ (increasing), ↓ (decreasing) and ⊗ (no trend); and significance level of the test (Sig.): α = 0.01(****), 0.05(***), 0.1(**) and 0.2(*). DJF (December, January, February), MAM (March, April, May), JJA (June, July, August), SON (September, October, November).

	N	Z	Sen yr^{-1} (%/yr)	CI	Trend	Sig.
DJF	12	2.95	0.0047 (0.9)	(0.0031, 0.0063)	↑	****
MAM	13	2.62	0.0030 (0.6)	(0.0018, 0.0046)	↑	****
JJA	11	2.67	0.0046 (0.9)	(0.0036, 0.0059)	↑	****
SON	12	2.81	0.0042 (0.8)	(0.0032, 0.0057)	↑	****
Annual	48	5.63	0.0042 (0.8)	(0.0036, 0.0049)	↑	****

the AAE are shown in Table 2. The AAE shows increasing trends for all seasons at the 99% confidence level, indicating a statistically significant upward trend, with a slope of 0.8%/yr. Generally, aerosol properties such as the AOD (Aerosol Optical Depth), the AE (Ångström Exponent) and the b_{abs} have also shown statistically significant decreasing trends in recent years, while the SSA (Single Scattering Albedo) and the b_{scat} generally exhibit increasing trends, but less spatially coherent (Li et al., 2014; Zhao et al., 2017; Collaud Coen et al., 2020a; Gupta et al., 2022). From measurements in the atmospheric column at our measurement site (AERONET station), Garcia-Suñer et al. (2023) found a statistically significant decreasing trend (at >80% confidence level) in AOD for most months; whereas the AE and the SSA do not show statistically significant long-term trends, only for a few months. The increasing trend in AAE is more complex to interpret compared to the trends observed in the eBC concentrations. AAE mainly depends on the chemical composition and properties of the particles, but particle size is also crucial, with larger particles generally being associated with lower AAE values (Schmeisser et al., 2017). For instance, an AAE greater than 2 corresponds to mineral dust for large particles and to BrC for smaller particles. Conversely, an AAE of less than 1 is linked to larger particles with low absorption, such as sea salt-dominant aerosols in the case of large particles and BC-dominant aerosols in smaller particles. A chemical analysis of the aerosols is crucial to accurately observe the modifications in the local atmospheric composition. In the absence of such data, the results shown in Table 2 may be attributed to changes in the dominant components of aerosols at the Burjassot site. The decrease observed in the eBC concentrations could suggest a higher relative abundance of other types of less absorbing particles in the last 12 years, contributing to an increase in the AAE.

4.3. Diurnal variability

The evolution during the day of the hourly eBC concentrations at Burjassot (weekdays and weekends separately) is shown in Fig. 6(a). The daily pattern exhibited by the eBC in Burjassot on weekdays is the typical shape reported in locations strongly influenced by traffic (Järvi et al., 2008; Reche et al., 2011; Mbengue et al., 2020; Luoma et al., 2021). The pattern is characterized by two daily peaks (07-09 LT and 19-21 LT) related to rush hours (Figure S7). The first peak is also related to atmospheric conditions which favor high concentrations: (a) the BLH is low and the air is stagnant, causing poor dispersion conditions; (b) the fumigation effect: the aerosols of the nocturnal residual layer mix with surface aerosols after sunrise. The eBC levels on weekends are lower and show a smoother pattern than weekdays levels, due to decreases of 70% and 30% in heavy and light traffic, respectively. The eBC concentrations during the weekend are highest during the early hours of the day. The reason could be that nighttime traffic intensity is higher on weekends (Figure S7). The minimum eBC concentrations at noon are related to the maximum daily BLH and wind speed (Figure S6), favoring pollutant dispersion, limiting near-surface stagnation and causing concentrations to decrease.

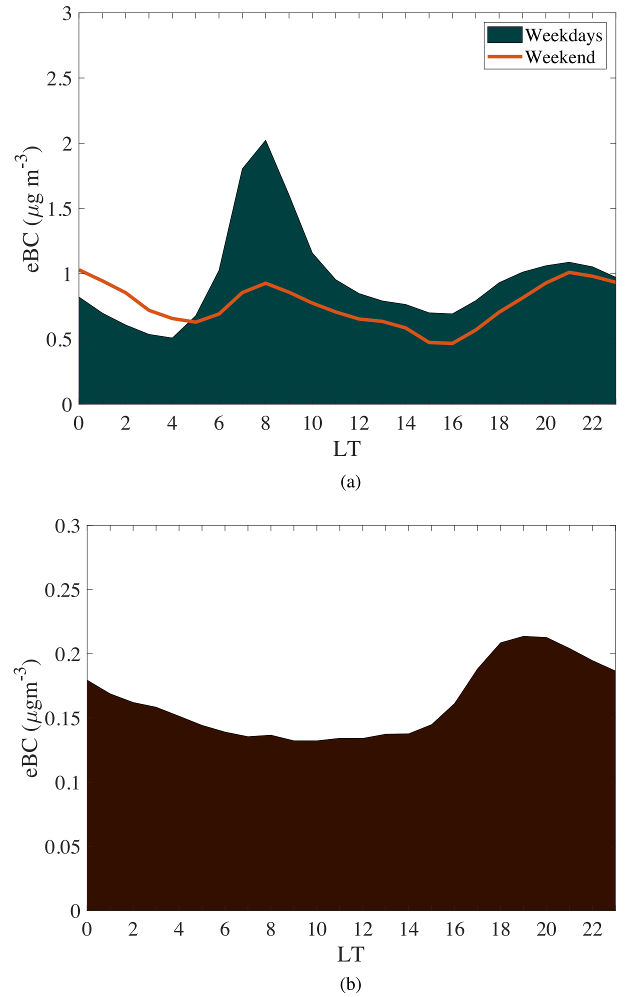

Fig. 6. Daily variability of eBC at (a) Burjassot (on weekdays and weekends) and (b) Aras de los Olmos sites.

The daily evolution of the hourly eBC concentrations at the Aras de los Olmos station is presented in Fig. 6(b). The concentration decreases gradually to a minimum value at 9–10 LT (around 0.13 μgm^{-3}) and begins to increase until the daily maximum occurs at about 19 LT. To explain this daily behavior, the local dynamics of the ABL should be taken into account. The BLH reaches its maximum daily value around 15–16 LT (Figure S8). The warming of the lower layers of the atmosphere causes pollutants that remain confined at low altitudes during the night to rise during the day. This ascent is determined by the BLH, so that a higher altitude will make it easier for pollutants to reach stations located at high altitudes. Pant et al. (2006), Nishita et al. (2007), Dumka et al. (2010), Motos et al. (2020) and Sun et al. (2021) have reported diurnal variations of eBC very similar to that seen in this study, attributing this to the boundary layer dynamics which brings up the polluted emissions from the underlying valley regions to the high altitude locations. In the case of Aras de los Olmos, there are no nearby sources of pollution, so transport must be from further away. Probably, the existence of the peak in the late afternoon has a close relationship with the wind speed and wind direction, since they govern the horizontal atmospheric transport. The next section is focused on the source identification based on the directional dependence of the highest concentrations.

4.3.1. Directional dependence of the daily pattern

Fig. 7 presents the CBPF diagrams using the 10-minute data of wind speed, wind direction and eBC concentration in the time interval 16–18

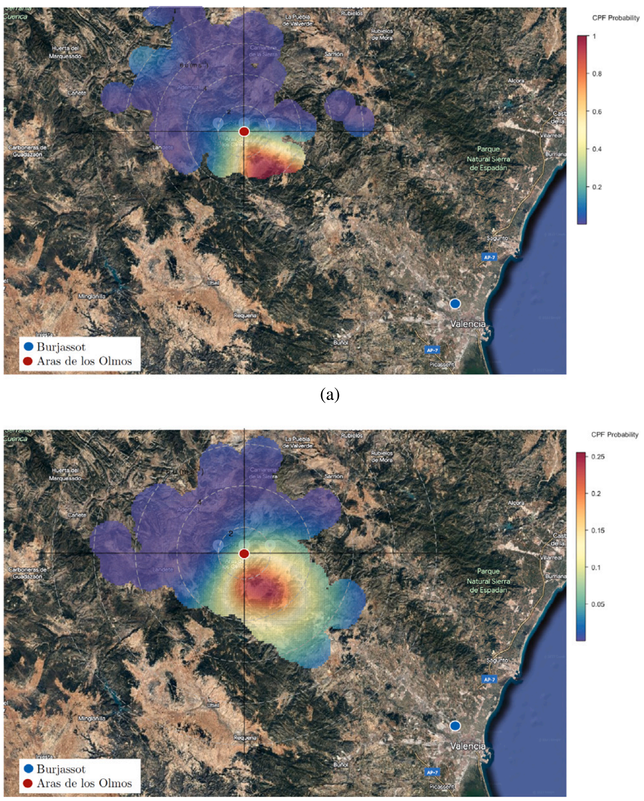

(a)

(b)

Fig. 7. CBPF diagrams at the Aras de los Olmos station using data at 16–18 LT during (a) winter and (b) summer superimposed on a map of both measurement sites and Valencia city. Wind speed is in m/s. The threshold value is the 75th percentile (0.14 μgm^{-3} and 0.37 μgm^{-3} in winter and summer, respectively).

LT separately in summer and winter. The CBPF are superimposed on a map illustrating the locations of both measurement sites and the urban center of Valencia. The reason for representing this time interval is that it coincides with the increase of concentrations in the daily pattern. In the absence of local emission sources, wind is expected to have a strong relevance on the daily eBC pattern.

There are some seasonal differences, especially in the directional distribution of the lower probabilities. During winter (Fig. 7(a)), there is a low contribution (CBPF < 0.2) from the northwest and with high wind speeds. However, the contribution from the southeast is predominant, with CBPF > 0.8. In summer (Fig. 7(b)), the highest concentrations also have a clear directional dependence. The city of Valencia, located 80 km southeast of the rural background station, seems to be the predominant origin of the particles arriving at the station.

5. Conclusions

The equivalent Black Carbon mass concentrations have been characterized for the first time at two locations in Valencia (Spain), representative of a metropolitan area of the city (Burjassot) and a background rural site (Aras de los Olmos). In-situ measurements from an AE-31 Aethalometer and a MAAP 5012 allowed to analyze this absorbing pollutant. This work includes the temporal characterization of the eBC concentrations, recognizing temporal patterns related to atmospheric variables and traffic, the identification of temporal trends and the analysis of the directional dependence. The main conclusions of this work are:

The average daily concentration (± standard deviation) for the entire measurement period (2011–2023) at the suburban site is 1.0 ± 0.5 μgm^{-3}, and varies considerably during the year, ranging from 0.7 ± 0.3 μgm^{-3} in June, July, and August to 1.4 ± 0.6 μgm^{-3} in December. This seasonal variability during the year is related to the seasonal evolution of the BLH. In addition, seasonal variability also depends on wind speed. The highest wind speed medians are reached in summer, allowing the horizontal dispersion. Both BLH and wind speed show higher variability in winter, which causes winter eBC concentrations to have higher daily variability.

The daily pattern of the eBC concentrations is marked by two peaks at 7–8 LT and around 20 LT, according to the evolution of traffic, especially on weekdays. The eBC levels on weekends are considerably reduced, which is consistent with the decrease in traffic. The minimum observed at midday is related to the maximum BLH caused by diurnal atmospheric dynamics, and not due to traffic, since it increases in that time frame.

Seasonal Mann–Kendall test and Sen's slope estimator were used to identify statistically significant trends of the eBC levels at the suburban site. The eBC concentrations exhibit increasing trends in all seasons of the year, being statistically significant for an 80% confidence level in winter, with a slope of −0.013 μgm^{-3}/yr or −5.0%/yr, and 99% for the other seasons, being the slopes −0.017 μgm^{-3}/yr or −9.8%/yr in spring, −0.020 μgm^{-3}/yr or −13.6%/yr in summer, and −0.032 μgm^{-3}/yr or −15.0%/yr in autumn. These decreasing trends are in general agreement with those observed in other European areas, especially in urban and metropolitan areas. The trends of eBC at the Burjassot site are also consistent with the Spanish National Inventory of Air Pollutants (Ministry for Ecological Transition and Demographic Challenge), according to which road transport-related BC emissions have been reduced by 42% since 2011.

Additionally, the MK test was conducted to analyze the long-term trends of the AAE. Statistically significant trends were observed for all seasonal medians at the 99% confidence level. The annual increase in the AAE may be associated with the observed decline in the eBC concentrations, which could allow other less absorbing aerosol types to become more dominant. In any case, a chemical analysis would be crucial to obtain more accurate information.

The daily concentrations (± standard deviation) of eBC at the rural background site during 2017–2023 vary annually from 0.08±0.05 μgm^{-3} in December to 0.23 ± 0.10 μgm^{-3} in August, being the average over the entire measurement period 0.17 ± 0.14 μgm^{-3}. Concentrations of eBC at Aras de los Olmos station vary during the year following the opposite pattern to that observed at the Burjassot station. The local anthropogenic influence is scarce, so the presence of BC particles is expected to be due to local emissions from biomass burning and the transport of pollution from the city of Valencia along the Turia river valley. The evolution of the BLH allows the particles to reach the station height (1280 m.a.s.l.). Wind speed also presents higher values in winter, in addition to greater variability. The lower wind speed in summer is related to situations of local stagnation, which favors higher concentrations.

The daily evolution of the eBC concentration in Aras de los Olmos is characterized by a slight decrease during the first hours of the day. From 9–10 LT the concentrations increase up to the daily maximum between 18 and 20 LT. This maximum could be due to the arrival of particles due to the vertical development of the mixing layer during the day. It may also be related to the daily transport of particles from population centers, which arrive at the measuring station at the end of the day. Using the CBPF polar diagrams, the predominant wind direction related to the daily highest eBC concentrations is southeast. Therefore, the presence of black carbon at the rural station depends on transportation from the city of Valencia (located 80 km to the southeast), following the Turia river valley.

The results of this study also reinforce the need to reduce black carbon emissions into the atmosphere. Additionally, it offers valuable information to support decision-making efforts aimed at improving the air quality in urban, suburban, and metropolitan areas. The implemented air quality regulations over the past years made possible the long-term reduction of pollutants observed on our sites, including BC. Therefore, in order to keep improving the air quality, we need to continue the effort to meet new WHO recommendations.

Based on the conclusions of this study, future research can proceed in two main directions: (1) to separate the contributions of traffic and biomass burning to eBC and (2) to quantify the influences of the different variables on the temporal variations of the concentrations at both measurement points.

CRediT authorship contribution statement

Violeta Matos: Writing – review & editing, Writing – original draft, Visualization, Validation, Software, Methodology, Investigation, Formal analysis, Conceptualization. **Víctor Estellés:** Writing – review & editing, Supervision, Software, Resources, Project administration, Methodology, Investigation, Funding acquisition, Data curation. **Josep Camarasa:** Software, Resources, Methodology, Investigation, Data curation. **Mar Sorribas:** Writing – review & editing, Validation, Supervision, Resources, Methodology, Investigation, Formal analysis, Conceptualization. **María Pilar Utrillas:** Writing – review & editing, Supervision, Project administration, Funding acquisition.

Declaration of competing interest

The authors declare that they have no known competing financial interests or personal relationships that could have appeared to influence the work reported in this paper.

Acknowledgments

This work was supported jointly by the Cience and Innovation Ministry, the State Research Agency and the European Regional Development Fund through projects PID2022-138730OB-I00, PID2021-123881OB-I00, TED2021-129185BI00 and PRE2018-084799; and by the Valencia Autonomous Government (Conselleria d'Educació, Cultura, Universitats i Ocupació) for the projects CIAICO2023-088, AICO/2021/341. We would like to acknowledge the local administration (Direcció General d' Obres Públiques, Transport i Mobilitat Sostenible de la Generalitat Valenciana) for the traffic data provided.

Appendix A. Acronyms and abbreviations

Description of acronyms and abbreviations used in the text.

AAE: Absorption Ångström Exponent

AAQD: Ambient Air Quality Directives

ABL: Atmospheric Boundary Layer

AE: Ångström Exponent

AOD: Aerosol Optical Depth

BASS: Burjassot AtmoSpheric Station

BC: Black Carbon

BLH: Boundary Layer Height

BrC: Brown Carbon

$\mathbf{b_{abs}}$: Absorption coefficient

$\mathbf{b_{atn}}$: Attenuation coefficient

$\mathbf{b_{scat}}$: Scattering coefficient

CBPF Conditional Bivariate Probability Function

CPF Conditional Probability Function

eBC: Equivalent Black Carbon

EC: Elemental Carbon

ECMWF: European Centre for Medium-Range Weather Forecast

IPCC: Intergovernmental Panel on Climate Change

LCA: Laboratorio de Contaminación Ambiental

LT: Local Time

MAAP: Multi-Angle Absorption Photometer

MAC: Mass Absorption Cross section

MK: Mann–Kendall

NIAP: National Inventory of Atmospheric Pollutants

OAO: Observatorio astronómico de Aras de los Olmos

PM: Particulate Matter

RF: Radiative Forcing

SSA: Single Scattering Albedo

WHO: World Health Organization

Appendix B. Supplementary data

Supplementary material related to this article can be found online at https://doi.org/10.1016/j.apr.2024.102367.

References

Arnott, W.P., Hamasha, K., Moosmüller, H., Sheridan, P.J., Ogren, J.A., 2005. Towards aerosol light-absorption measurements with a 7-wavelength aethalometer: Evaluation with a photoacoustic instrument and 3-wavelength nephelometer. Aerosol Sci. Technol. 39 (1), 17–29. http://dx.doi.org/10.1080/027868290901972.

Becerril-Valle, M., Coz, E., Prévôt, A., Močnik, G., Pandis, S., Sánchez de la Campa, A., Alastuey, A., Díaz, E., Pérez, R., Artíñano, B., 2017. Characterization of atmospheric black carbon and co-pollutants in urban and rural areas of Spain. Atmos. Environ. 169, 36–53. http://dx.doi.org/10.1016/j.atmosenv.2017.09.014, URL: https://www.sciencedirect.com/science/article/pii/S1352231017306052.

Beelen, R., Hoek, G., van den Brandt, P.A., Goldbohm, R.A., Fischer, P., Schouten, L.J., Jerrett, M., Hughes, E., Armstrong, B., Brunekreef, B., 2008. Long-term effects of traffic-related air pollution on mortality in a dutch cohort (NLCS-AIR study). Environ. Health Perspect. 116 (2), 196–202. http://dx.doi.org/10.1289/ehp.10767, URL: https://ehp.niehs.nih.gov/doi/abs/10.1289/ehp.10767.

Bernstein, J.A., Alexis, N., Barnes, C., Bernstein, I.L., Nel, A., Peden, D., Diaz-Sanchez, D., Tarlo, S.M., Williams, P.B., Bernstein, J.A., 2004. Health effects of air pollution. J. Allergy Clin. Immunol. 114 (5), 1116–1123. http://dx.doi.org/10.1016/j.jaci.2004.08.030, URL: https://www.sciencedirect.com/science/article/pii/S0091674904022663.

Bond, T.C., Bergstrom, R.W., 2006. Light absorption by carbonaceous particles: An investigative review. Aerosol Sci. Technol. 40 (1), 27–67. http://dx.doi.org/10.1080/02786820500421521.

Bond, T.C., Doherty, S.J., Fahey, D.W., Forster, P.M., Berntsen, T., DeAngelo, B.J., Flanner, M.G., Ghan, S., Kärcher, B., Koch, D., Kinne, S., Kondo, Y., Quinn, P.K., Sarofim, M.C., Schultz, M.G., Schulz, M., Venkataraman, C., Zhang, H., Zhang, S., Bellouin, N., Guttikunda, S.K., Hopke, P.K., Jacobson, M.Z., Kaiser, J.W., Klimont, Z., Lohmann, U., Schwarz, J.P., Shindell, D., Storelvmo, T., Warren, S.G., Zender, C.S., 2013. Bounding the role of black carbon in the climate system: A scientific assessment. J. Geophys. Res.: Atmos. 118 (11), 5380–5552. http://dx.doi.org/10.1002/jgrd.50171.

Bond, T.C., Habib, G., Bergstrom, R.W., 2006. Limitations in the enhancement of visible light absorption due to mixing state. J. Geophys. Res.: Atmos. 111 (D20), http://dx.doi.org/10.1029/2006JD007315.

Carslaw, D., 2018. The openair manual - open source tools for analysing air pollution data (12th version). Universidad de York, Reino Unido.
Carslaw, D.C., Ropkins, K., 2012. Openair — An R package for air quality data analysis. Environ. Model. Softw. 27–28, 52–61. http://dx.doi.org/10.1016/j.envsoft.2011.09.008.
Casquero-Vera, J., Lyamani, H., Titos, G., Minguillón, M., Dada, L., Alastuey, A., Querol, X., Petäjä, T., Olmo, F., Alados-Arboledas, L., 2021. Quantifying traffic, biomass burning and secondary source contributions to atmospheric particle number concentrations at urban and suburban sites. Sci. Total Environ. 768, 145282. http://dx.doi.org/10.1016/j.scitotenv.2021.145282, URL: https://www.sciencedirect.com/science/article/pii/S004896972100348X.
Collaud Coen, M., Andrews, E., Alastuey, A., Arsov, T.P., Backman, J., Brem, B.T., Bukowiecki, N., Couret, C., Eleftheriadis, K., Flentje, H., Fiebig, M., Gysel-Beer, M., Hand, J.L., Hoffer, A., Hooda, R., Hueglin, C., Joubert, W., Keywood, M., Kim, J.E., Kim, S.-W., Labuschagne, C., Lin, N.-H., Lin, Y., Lund Myhre, C., Luoma, K., Lyamani, H., Marinoni, A., Mayol-Bracero, O.L., Mihalopoulos, N., Pandolfi, M., Prats, N., Prenni, A.J., Putaud, J.-P., Ries, L., Reisen, F., Sellegri, K., Sharma, S., Sheridan, P., Sherman, J.P., Sun, J., Titos, G., Torres, E., Tuch, T., Weller, R., Wiedensohler, A., Zieger, P., Laj, P., 2020a. Multidecadal trend analysis of in situ aerosol radiative properties around the world. Atmos. Chem. Phys. 20 (14), 8867–8908. http://dx.doi.org/10.5194/acp-20-8867-2020.
Collaud Coen, M., Andrews, E., Asmi, A., Baltensperger, U., Bukowiecki, N., Day, D., Fiebig, M., Fjaeraa, A.M., Flentje, H., Hyvärinen, A., Jefferson, A., Jennings, S.G., Kouvarakis, G., Lihavainen, H., Lund Myhre, C., Malm, W.C., Mihapopoulos, N., Molenar, J.V., O'Dowd, C., Ogren, J.A., Schichtel, B.A., Sheridan, P., Virkkula, A., Weingartner, E., Weller, R., Laj, P., 2013. Aerosol decadal trends – part 1: In-situ optical measurements at GAW and IMPROVE stations. Atmos. Chem. Phys. 13 (2), 869–894. http://dx.doi.org/10.5194/acp-13-869-2013.
Collaud Coen, M., Andrews, E., Bigi, A., Martucci, G., Romanens, G., Vogt, F.P.A., Vuilleumier, L., 2020b. Effects of the prewhitening method, the time granularity, and the time segmentation on the Mann–Kendall trend detection and the associated Sen's slope. Atmos. Meas. Tech. 13 (12), 6945–6964. http://dx.doi.org/10.5194/amt-13-6945-2020.
Collaud Coen, M., Weingartner, E., Apituley, A., Ceburnis, D., Fierz-Schmidhauser, R., Flentje, H., Henzing, J.S., Jennings, S.G., Moerman, M., Petzold, A., Schmid, O., Baltensperger, U., 2010. Minimizing light absorption measurement artifacts of the aethalometer: evaluation of five correction algorithms. Atmos. Meas. Tech. 3 (2), 457–474. http://dx.doi.org/10.5194/amt-3-457-2010, URL: https://amt.copernicus.org/articles/3/457/2010/.
Council of the European Union, 2023. Proposal for a Directive of the European Parliament and of the Council on Ambient Air Quality and Cleaner Air for Europe (Recast), Mandate for Negotiations with the European Parliament. Brussels.
Ding, A.J., Huang, X., Nie, W., Sun, J.N., Kerminen, V.-M., Petäjä, T., Su, H., Cheng, Y.F., Yang, X.-Q., Wang, M.H., Chi, X.G., Wang, J.P., Virkkula, A., Guo, W.D., Yuan, J., Wang, S.Y., Zhang, R.J., Wu, Y.F., Song, Y., Zhu, T., Zilitinkevich, S., Kulmala, M., Fu, C.B., 2016. Enhanced haze pollution by black carbon in megacities in China. Geophys. Res. Lett. 43 (6), 2873–2879. http://dx.doi.org/10.1002/2016GL067745, URL: https://agupubs.onlinelibrary.wiley.com/doi/abs/10.1002/2016GL067745.
Dumka, U., Moorthy, K.K., Kumar, R., Hegde, P., Sagar, R., Pant, P., Singh, N., Babu, S.S., 2010. Characteristics of aerosol black carbon mass concentration over a high altitude location in the central himalayas from multi-year measurements. Atmos. Res. 96 (4), 510–521. http://dx.doi.org/10.1016/j.atmosres.2009.12.010, URL: https://www.sciencedirect.com/science/article/pii/S0169809509003494.
EEA, 2022. EEA Environmental Statement 2021 Report. Technical Report, European Environmental Agency, Copenhagen, Denmark, http://dx.doi.org/10.2800/2114.
Estellés, V., Martínez-Lozano, J.A., Utrillas, M.P., Campanelli, M., 2007. Columnar aerosol properties in Valencia (Spain) by ground-based Sun photometry. J. Geophys. Res.: Atmos. 112 (D11), http://dx.doi.org/10.1029/2006JD008167, arXiv:https://agupubs.onlinelibrary.wiley.com/doi/pdf/10.1029/2006JD008167.
Estellés, V., Utrillas, M.P., Martínez-Lozano, J.A., 2005. Study of a pollution episode in valencia (Spain) due to biomass fires in 'La Albufera' rice paddies. In: Proceedings of the 5th International Conference on Urban Air Quality.
Esteve, A.R., Estellés, V., Segura, S., Utrillas, M., Martínez-Lozano, J.A., 2012a. Influence of the trajectory of air masses on the in situ measurements of aerosol properties in valencia. Tethys J. Weather Clim. West. Mediterranean 9, 35–41. http://dx.doi.org/10.3369/tethys.2012.9.04.
Esteve, A.R., Estellés, V., Utrillas, M.P., Martínez-Lozano, J.A., 2012b. In-situ integrating nephelometer measurements of the scattering properties of atmospheric aerosols at an urban coastal site in western Mediterranean. Atmos. Environ. 47, 43–50. http://dx.doi.org/10.1016/j.atmosenv.2011.11.043, URL: https://www.sciencedirect.com/science/article/pii/S1352231011012295.
Evangeliou, N., Platt, S.M., Eckhardt, S., Lund Myhre, C., Laj, P., Alados-Arboledas, L., Backman, J., Brem, B.T., Fiebig, M., Flentje, H., Marinoni, A., Pandolfi, M., Yus-Dìez, J., Prats, N., Putaud, J.P., Sellegri, K., Sorribas, M., Eleftheriadis, K., Vratolis, S., Wiedensohler, A., Stohl, A., 2021. Changes in black carbon emissions over europe due to COVID-19 lockdowns. Atmos. Chem. Phys. 21 (4), 2675–2692. http://dx.doi.org/10.5194/acp-21-2675-2021.
Farzad, K., Khorsandi, B., Khorsandi, M., Bouamra, O., Maknoon, R., 2020. A study of cardiorespiratory related mortality as a result of exposure to black carbon. Sci. Total Environ. 725, 138422. http://dx.doi.org/10.1016/j.scitotenv.2020.138422.
Freire, C., Ramos, R., Puertas, R., Lopez-Espinosa, M.-J., Julvez, J., Aguilera, I., Cruz-Quintana, F., Fernández, M., Sunyer, J., Olea, N., 2010. Association of traffic-related air pollution with cognitive development in children. J. Epidemiol. Community Health 64, 223–228. http://dx.doi.org/10.1136/jech.2008.084574.
Fuller, K.A., Malm, W.C., Kreidenweis, S.M., 1999. Effects of mixing on extinction by carbonaceous particles. J. Geophys. Res.: Atmos. 104 (D13), 15941–15954. http://dx.doi.org/10.1029/1998JD100069, arXiv:https://agupubs.onlinelibrary.wiley.com/doi/pdf/10.1029/1998JD100069.
Garcia-Suñer, M., Matos, V., Kumar, G., Estellés, V., Utrillas, M., 2023. 20 years of columnar aerosol properties at valencia area (Eastern Spain) by ground-based sun-photometry. Atmos. Res. 1, 1. http://dx.doi.org/10.1016/j.atmosres.2023.107198.
Gilbert, R.O., 1987. Statistical Methods for Environmental Pollution Monitoring. Wiley, New York, USA, p. 336.
Gómez-Amo, J., Estellés, V., Marcos, C., Segura, S., Esteve, A., Pedrós, R., Utrillas, M., Martínez-Lozano, J., 2017. Impact of dust and smoke mixing on column-integrated aerosol properties from observations during a severe wildfire episode over Valencia (Spain). Sci. Total Environ. 599–600, 2121–2134. http://dx.doi.org/10.1016/j.scitotenv.2017.05.041.
Gupta, G., Venkat Ratnam, M., Madhavan, B., Narayanamurthy, C., 2022. Long-term trends in Aerosol Optical Depth obtained across the globe using multi-satellite measurements. Atmos. Environ. 273, 118953. http://dx.doi.org/10.1016/j.atmosenv.2022.118953, URL: https://www.sciencedirect.com/science/article/pii/S1352231022000188.
Hansen, A.D.A., 2005. The Aethalometer. Magee Scientific Company, Berkeley, California, USA.
Healy, R., Sofowote, U., Su, Y., Debosz, J., Noble, M., Jeong, C.-H., Wang, J., Hilker, N., Evans, G., Doerksen, G., Jones, K., Munoz, A., 2017. Ambient measurements and source apportionment of fossil fuel and biomass burning black carbon in Ontario. Atmos. Environ. 161, 34–47. http://dx.doi.org/10.1016/j.atmosenv.2017.04.034, URL: https://www.sciencedirect.com/science/article/pii/S1352231017302789.
Helin, A., Niemi, J.V., Virkkula, A., Pirjola, L., Teinilä, K., Backman, J., Aurela, M., Saarikoski, S., Rönkkö, T., Asmi, E., Timonen, H., 2018. Characteristics and source apportionment of black carbon in the Helsinki metropolitan area, Finland. Atmos. Environ. 190, 87–98. http://dx.doi.org/10.1016/j.atmosenv.2018.07.022, URL: https://www.sciencedirect.com/science/article/pii/S1352231018304692.
Hersbach, H., Bell, B., Berrisford, P., Hirahara, S., Horányi, A., Muñoz-Sabater, J., Nicolas, J., Peubey, C., Radu, R., Schepers, D., Simmons, A., Soci, C., Abdalla, S., Abellan, X., Balsamo, G., Bechtold, P., Biavati, G., Bidlot, J., Bonavita, M., De Chiara, G., Dahlgren, P., Dee, D., Diamantakis, M., Dragani, R., Flemming, J., Forbes, R., Fuentes, M., Geer, A., Haimberger, L., Healy, S., Hogan, R.J., Hólm, E., Janisková, M., Keeley, S., Laloyaux, P., Lopez, P., Lupu, C., Radnoti, G., de Rosnay, P., Rozum, I., Vamborg, F., Villaume, S., Thépaut, J.-N., 2020. The ERA5 global reanalysis. Q. J. R. Meteorol. Soc. 146 (730), 1999–2049. http://dx.doi.org/10.1002/qj.3803, URL: https://rmets.onlinelibrary.wiley.com/doi/abs/10.1002/qj.3803.
Hirsch, R., Slack, J., Smith, R., 1982. Techniques of trend analysis for monthly water quality data. Water Resour. Res. 18, 107–121. http://dx.doi.org/10.1029/WR018i001p00107.
Hu, Y., Kang, S., Yang, J., Chen, X., Ji, Z., Rai, M., 2022. Transport of black carbon from central and west Asia to the Tibetan Plateau: Seasonality and climate effect. Atmos. Res. 267, 105987. http://dx.doi.org/10.1016/j.atmosres.2021.105987, URL: https://www.sciencedirect.com/science/article/pii/S0169809521005433.
IPCC, 2021. In: Masson-Delmotte, V., Zhai, P., Pirani, A., Connors, S.L., Péan, C., Berger, S., Caud, N., Chen, Y., Goldfarb, L., Gomis, M.I., Huang, M., Leitzell, K., Lonnoy, E., Matthews, J.B.R., Maycock, T.K., Waterfield, T., Yelekçi, O., Yu, R., Zhou, B. (Eds.), Climate Change 2021: The Physical Science Basis. Contribution of Working Group I to the Sixth Assessment Report of the Intergovernmental Panel on Climate Change. Cambridge University Press, Cambridge, United Kindom and New York, NY, USA, p. 2391. http://dx.doi.org/10.1017/9781009157896.
Janssen, N.A., Hoek, G., Simic-Lawson, M., Fischer, P., van Bree, L., ten Brink, H., Keuken, M., Atkinson, R.W., Anderson, H.R., Brunekreef, B., Cassee, F.R., 2011. Black carbon as an additional indicator of the adverse health effects of airborne particles compared with PM_{10} and $PM_{2.5}$. Environ. Health Perspect. 119 (12), 1691–1699. http://dx.doi.org/10.1289/ehp.1003369.
Järvi, L., Junninen, H., Karppinen, A., Hillamo, R., Virkkula, A., Mäkelä, T., Pakkanen, T., Kulmala, M., 2008. Temporal variations in black carbon concentrations with different time scales in Helsinki during 1996–2005. Atmos. Chem. Phys. 8 (4), 1017–1027. http://dx.doi.org/10.5194/acp-8-1017-2008, URL: https://acp.copernicus.org/articles/8/1017/2008/.
Ji, Z.-M., 2016. Modeling black carbon and its potential radiative effects over the tibetan plateau. Adv. Clim. Change Res. 7 (3), 139–144. http://dx.doi.org/10.1016/j.accre.2016.10.002, URL: https://www.sciencedirect.com/science/article/pii/S1674927816300430.
Jia, M., Evangeliou, N., Eckhardt, S., Huang, X., Gao, J., Ding, A., Stohl, A., 2021. Black carbon emission reduction due to COVID-19 lockdown in China. Geophys. Res. Lett. 48, http://dx.doi.org/10.1029/2021GL093243.
Kanakidou, M., Seinfeld, J.H., Pandis, S.N., Barnes, I., Dentener, F.J., Facchini, M.C., Van Dingenen, R., Ervens, B., Nenes, A., Nielsen, C.J., Swietlicki, E., Putaud, J.P., Balkanski, Y., Fuzzi, S., Horth, J., Moortgat, G.K., Winterhalter, R., Myhre, C.E.L.,

Tsigaridis, K., Vignati, E., Stephanou, E.G., Wilson, J., 2005. Organic aerosol and global climate modelling: a review. Atmos. Chem. Phys. 5 (4), 1053–1123. http://dx.doi.org/10.5194/acp-5-1053-2005.

Kang, S., Zhang, Y., Qian, Y., Wang, H., 2020. A review of black carbon in snow and ice and its impact on the cryosphere. Earth-Sci. Rev. 210, 103346. http://dx.doi.org/10.1016/j.earscirev.2020.103346, URL: https://www.sciencedirect.com/science/article/pii/S0012825220303925.

Kendall, M.G., 1975. Rank Correlation Methods, fourth ed. Charles Griffin, London.

Koch, D., Del Genio, A.D., 2010. Black carbon semi-direct effects on cloud cover: review and synthesis. Atmos. Chem. Phys. 10 (16), 7685–7696. http://dx.doi.org/10.5194/acp-10-7685-2010, URL: https://acp.copernicus.org/articles/10/7685/2010/.

Lee, W.-L., Liou, K., He, C., Liang, H.-C., Wang, T.-C., Li, Q., Liu, Z., Yue, Q., 2017. Impact of absorbing aerosol deposition on snow albedo reduction over the southern Tibetan plateau based on satellite observations. Theor. Appl. Climatol. 129, 1373–1382.

Li, J., Carlson, B.E., Dubovik, O., Lacis, A.A., 2014. Recent trends in aerosol optical properties derived from AERONET measurements. Atmos. Chem. Phys. 14 (22), 12271–12289. http://dx.doi.org/10.5194/acp-14-12271-2014.

Li, Y., Henze, D.K., Jack, D., Henderson, B.H., Kinney, P.L., 2016. Assessing public health burden associated with exposure to ambient black carbon in the United States. Sci. Total Environ. 539, 515–525. http://dx.doi.org/10.1016/j.scitotenv.2015.08.129, URL: https://www.sciencedirect.com/science/article/pii/S0048969715306318.

Ljungman, P.L., Andersson, N., Stockfelt, L., Andersson, E.M., Nilsson Sommar, J., Eneroth, K., Gidhagen, L., Johansson, C., Lager, A., Leander, K., et al., 2019. Long-term exposure to particulate air pollution, black carbon, and their source components in relation to ischemic heart disease and stroke. Environ. Health Perspect. 127 (10), 107012. http://dx.doi.org/10.1289/EHP4757.

Lohmann, U., Feichter, J., 2005. Global indirect aerosol effects: a review. Atmospheric Chem. Phys. 5 (3), 715–737. http://dx.doi.org/10.5194/acp-5-715-2005, URL: https://acp.copernicus.org/articles/5/715/2005/.

López-Caravaca, A., Nicolás, J., Lucarelli, F., Castañer, R., Crespo, J., Galindo, N., Calzolai, G., Yubero, E., Clemente, A., Pazzi, G., 2022. Combination of PM optical and chemical properties to estimate the contribution of non-BC absorbers to light absorption at a remote site. Atmos. Res. 268, 106000. http://dx.doi.org/10.1016/j.atmosres.2021.106000, URL: https://www.sciencedirect.com/science/article/pii/S0169809521005561.

Luoma, K., Niemi, J.V., Aurela, M., Fung, P.L., Helin, A., Hussein, T., Kangas, L., Kousa, A., Rönkkö, T., Timonen, H., Virkkula, A., Petäjä, T., 2021. Spatiotemporal variation and trends in equivalent black carbon in the helsinki metropolitan area in Finland. Atmos. Chem. Phys. 21 (2), 1173–1189. http://dx.doi.org/10.5194/acp-21-1173-2021, URL: https://acp.copernicus.org/articles/21/1173/2021/.

Mann, H.B., 1945. Nonparametric tests against trend. Econometrica 13 (3), 245–259, URL: http://www.jstor.org/stable/1907187.

Matos, V., Camarasa, J., Segura, S., Estellés, V., Utrillas, M.P., Martínez-Lozano, J.A., 2020. Poster: Multitemporal analysis of black carbon at two urban and blackground locations in Valencia (Spain). In: European Aerosol Conference. EAC.

Mbengue, S., Serfozo, N., Schwarz, J., Ziková, N., Šmejkalová, A.H., Holoubek, I., 2020. Characterization of equivalent black carbon at a regional background site in Central Europe: Variability and source apportionment. Environ. Pollut. 260, 113771. http://dx.doi.org/10.1016/j.envpol.2019.113771, URL: https://www.sciencedirect.com/science/article/pii/S0269749119328477.

Motos, G., Corbin, J.C., Schmale, J., Modini, R.L., Bertò, M., Kupiszewski, P., Baltensperger, U., Gysel-Beer, M., 2020. Black carbon aerosols in the lower free troposphere are heavily coated in summer but largely uncoated in winter at jungfraujoch in the swiss alps. Geophys. Res. Lett. 47 (14), e2020GL088011. http://dx.doi.org/10.1029/2020GL088011.

Müller, T., Henzing, B., de Leeuw, G., Wiedensohler, A., Alastuey, A., Angelov, C., Bizjak, M., Collaud Coen, M., Engström, J., Gruening, C., Hillamo, R., Hoffer, A., Imre, K., Ivanow, P., Jennings, G., Sun, J., Kalivitis, N., Karlsson, H., Komppula, M., Wang, Y., 2011. Characterization and intercomparison of aerosol absorption photometers: Result of two intercomparison workshops. Atmos. Meas. Tech. 4, 245–268. http://dx.doi.org/10.5194/amtd-3-1511-2010.

Nicolás, J., Castañer, R., Crespo, J., Yubero, E., Galindo, N., Pastor, C., 2018. Seasonal variability of aerosol absorption parameters at a remote site with high mineral dust loads. Atmos. Res. 210, 100–109. http://dx.doi.org/10.1016/j.atmosres.2018.04.008.

Nishita, C., Osada, K., Matsunaga, K., Iwasaka, Y., 2007. Number-size distributions of free tropospheric aerosol particles at Mt. Norikura, Japan: Effects of precipitation and air mass transportation pathways. J. Geophys. Res.: Atmos. 112 (D10), http://dx.doi.org/10.1029/2006JD007969.

Pant, P., Hegde, P., Dumka, U.C., Sagar, R., Satheesh, S.K., Moorthy, K.K., Saha, A., Srivastava, M.K., 2006. Aerosol characteristics at a high-altitude location in central himalayas: Optical properties and radiative forcing. J. Geophys. Res.: Atmos. 111 (D17), http://dx.doi.org/10.1029/2005JD006768.

Peters, R., Ee, N., Peters, J., Booth, A., Mudway, I., Anstey, K.J., 2019. Air pollution and dementia: a systematic review. J. Alzheimer's Dis. 70 (s1), S145–S163.

Petzold, A., Ogren, J.A., Fiebig, M., Laj, P., Li, S.-M., Baltensperger, U., Holzer-Popp, T., Kinne, S., Pappalardo, G., Sugimoto, N., Wehrli, C., Wiedensohler, A., Zhang, X.-Y., 2013. Recommendations for reporting "black carbon" measurements. Atmos. Chem. Phys. 13 (16), 8365–8379. http://dx.doi.org/10.5194/acp-13-8365-2013, URL: https://acp.copernicus.org/articles/13/8365/2013/.

Petzold, A., Schönlinner, M., 2004. Multi-angle absorption photometry—a new method for the measurement of aerosol light absorption and atmospheric black carbon. J. Aerosol Sci. 35 (4), 421–441. http://dx.doi.org/10.1016/j.jaerosci.2003.09.005, URL: https://www.sciencedirect.com/science/article/pii/S0021850203004403.

Power, M., Weisskopf, M., Alexeeff, S., Coull, B., Spiro, A., Schwartz, J., 2011. Traffic-related air pollution and cognitive function in a cohort of older men. Environ. Health Perspect. 119, 682–687.

Putaud, J.-P., Van Dingenen, R., Alastuey, A., Bauer, H., Birmili, W., Cyrys, J., Flentje, H., Fuzzi, S., Gehrig, R., Hansson, H., Harrison, R., Herrmann, H., Hitzenberger, R., Hüglin, C., Jones, A., Kasper-Giebl, A., Kiss, G., Kousa, A., Kuhlbusch, T., Löschau, G., Maenhaut, W., Molnar, A., Moreno, T., Pekkanen, J., Perrino, C., Pitz, M., Puxbaum, H., Querol, X., Rodriguez, S., Salma, I., Schwarz, J., Smolik, J., Schneider, J., Spindler, G., ten Brink, H., Tursic, J., Viana, M., Wiedensohler, A., Raes, F., 2010. A European aerosol phenomenology – 3: Physical and chemical characteristics of particulate matter from 60 rural, urban, and kerbside sites across europe. Atmos. Environ. 44 (10), 1308–1320. http://dx.doi.org/10.1016/j.atmosenv.2009.12.011, URL: https://www.sciencedirect.com/science/article/pii/S1352231009010358.

Rajesh, T., Ramachandran, S., 2022. Assessment of the coronavirus disease 2019 (COVID-19) pandemic imposed lockdown and unlock effects on black carbon aerosol, its source apportionment, and aerosol radiative forcing over an urban city in India. Atmos. Res. 267, 105924. http://dx.doi.org/10.1016/j.atmosres.2021.105924, URL: https://www.sciencedirect.com/science/article/pii/S0169809521004804.

Reche, C., Querol, X., Alastuey, A., Viana, M., Pey, J., Moreno, T., Rodríguez, S., González, Y., Fernández-Camacho, R., de la Rosa, J., Dall'Osto, M., Prèvôt, A.S.H., Hueglin, C., Harrison, R.M., Quincey, P., 2011. New considerations for PM, black carbon and particle number concentration for air quality monitoring across different European cities. Atmos. Chem. Phys. 11 (13), 6207–6227. http://dx.doi.org/10.5194/acp-11-6207-2011, URL: https://acp.copernicus.org/articles/11/6207/2011/.

Saarikoski, S., Niemi, J.V., Aurela, M., Pirjola, L., Kousa, A., Rönkkö, T., Timonen, H., 2021. Sources of black carbon at residential and traffic environments obtained by two source apportionment methods. Atmos. Chem. Phys. 21 (19), 14851–14869. http://dx.doi.org/10.5194/acp-21-14851-2021, URL: https://acp.copernicus.org/articles/21/14851/2021/.

Sand, M., Samset, B.H., Tsigaridis, K., Bauer, S.E., Myhre, G., 2020. Black carbon and precipitation: An energetics perspective. J. Geophys. Res.: Atmos. 125 (13), e2019JD032239. http://dx.doi.org/10.1029/2019JD032239.

Sandradewi, J., Prévôt, A., Weingartner, E., Schmidhauser, R., Gysel, M., Baltensperger, U., 2008. A study of wood burning and traffic aerosols in an alpine valley using a multi-wavelength aethalometer, xurl= https://www.sciencedirect.com/science/article/pii/S1352231007008072. Atmos. Environ. 42 (1), 101–112. http://dx.doi.org/10.1016/j.atmosenv.2007.09.034.

Savadkoohi, M., Pandolfi, M., Reche, C., Niemi, J.V., Mooibroek, D., Titos, G., Green, D.C., Tremper, A.H., Hueglin, C., Liakakou, E., Mihalopoulos, N., Stavroulas, I., Artiñano, B., Coz, E., Alados-Arboledas, L., Beddows, D., Riffault, V., De Brito, J.F., Bastian, S., Baudic, A., Colombi, C., Costabile, F., Chazeau, B., Marchand, N., Gómez-Amo, J.L., Estellés, V., Matos, V., van der Gaag, E., Gille, G., Luoma, K., Manninen, H.E., Norman, M., Silvergren, S., Petit, J.-E., Putaud, J.-P., Rattigan, O.V., Timonen, H., Tuch, T., Merkel, M., Weinhold, K., Vratolis, S., Vasilescu, J., Favez, O., Harrison, R.M., Laj, P., Wiedensohler, A., Hopke, P.K., Petäjä, T., Alastuey, A., Querol, X., 2023. The variability of mass concentrations and source apportionment analysis of equivalent black carbon across urban Europe. Environ. Int. 178, 108081. http://dx.doi.org/10.1016/j.envint.2023.108081, URL: https://www.sciencedirect.com/science/article/pii/S0160412023003549.

Schmeisser, L., Andrews, E., Ogren, J.A., Sheridan, P., Jefferson, A., Sharma, S., Kim, J.E., Sherman, J.P., Sorribas, M., Kalapov, I., Arsov, T., Angelov, C., Mayol-Bracero, O.L., Labuschagne, C., Kim, S.-W., Hoffer, A., Lin, N.-H., Chia, H.-P., Bergin, M., Sun, J., Liu, P., Wu, H., 2017. Classifying aerosol type using in situ surface spectral aerosol optical properties. Atmos. Chem. Phys. 17 (19), 12097–12120. http://dx.doi.org/10.5194/acp-17-12097-2017.

Schmid, O., Artaxo, P., Arnott, W.P., Chand, D., Gatti, L.V., Frank, G.P., Hoffer, A., Schnaiter, M., Andreae, M.O., 2006. Spectral light absorption by ambient aerosols influenced by biomass burning in the Amazon Basin. I: Comparison and field calibration of absorption measurement techniques. Atmos. Chem. Phys. 6 (11), 3443–3462. http://dx.doi.org/10.5194/acp-6-3443-2006, URL: https://acp.copernicus.org/articles/6/3443/2006/.

Schnaiter, M., Linke, C., Möhler, O., Naumann, K.-H., Saathoff, H., Wagner, R., Schurath, U., Wehner, B., 2005. Absorption amplification of black carbon internally mixed with secondary organic aerosol. J. Geophys. Res.: Atmos. 110 (D19), http://dx.doi.org/10.1029/2005JD006046, URL: https://agupubs.onlinelibrary.wiley.com/doi/abs/10.1029/2005JD006046.

Sciare, J., d'Argouges, O., Sarda-Estève, R., Gaimoz, C., Dolgorouky, C., Bonnaire, N., Favez, O., Bonsang, B., Gros, V., 2011. Large contribution of water-insoluble secondary organic aerosols in the region of Paris (France) during wintertime. J. Geophys. Res.: Atmos. 116 (D22), 1–24.

Segura, S., Estellés, V., Esteve, A., Marcos, C., Utrillas, M., Martínez-Lozano, J., 2016. Multiyear in-situ measurements of atmospheric aerosol absorption properties at an urban coastal site in western Mediterranean. Atmos. Environ. 129, 18–26. http://dx.doi.org/10.1016/j.atmosenv.2016.01.008, URL: https://www.sciencedirect.com/science/article/pii/S1352231016300085.

Segura, S., Estellés, V., Titos, G., Lyamani, H., Utrillas, M.P., Zotter, P., Prèvôt, A.S.H., Močnik, G., Alados-Arboledas, L., Martínez-Lozano, J.A., 2014. Determination and analysis of in situ spectral aerosol optical properties by a multi-instrumental approach. Atmos. Meas. Tech. 7 (8), 2373–2387. http://dx.doi.org/10.5194/amt-7-2373-2014, URL: https://amt.copernicus.org/articles/7/2373/2014/.

Sen, P.K., 1968. Estimates of the regression coefficient based on Kendall's Tau. J. Amer. Statist. Assoc. 63 (324), 1379–1389. http://dx.doi.org/10.1080/01621459.1968.10480934.

Shivani, Gadi, R., Sharma, S.K., Mandal, T.K., 2019. Seasonal variation, source apportionment and source attributed health risk of fine carbonaceous aerosols over National Capital Region, India. Chemosphere 237, 124500. http://dx.doi.org/10.1016/j.chemosphere.2019.124500, URL: https://www.sciencedirect.com/science/article/pii/S0045653519317242.

Spracklen, D.V., Carslaw, K.S., Pöschl, U., Rap, A., Forster, P.M., 2011. Global cloud condensation nuclei influenced by carbonaceous combustion aerosol. Atmos. Chem. Phys. 11 (17), 9067–9087. http://dx.doi.org/10.5194/acp-11-9067-2011, URL: https://acp.copernicus.org/articles/11/9067/2011/.

Sun, J., Birmili, W., Hermann, M., Tuch, T., Weinhold, K., Merkel, M., Rasch, F., Müller, T., Schladitz, A., Bastian, S., Löschau, G., Cyrys, J., Gu, J., Flentje, H., Briel, B., Asbach, C., Kaminski, H., Ries, L., Sohmer, R., Gerwig, H., Wirtz, K., Meinhardt, F., Schwerin, A., Bath, O., Ma, N., Wiedensohler, A., 2020. Decreasing trends of particle number and black carbon mass concentrations at 16 observational sites in Germany from 2009 to 2018. Atmos. Chem. Phys. 20 (11), 7049–7068. http://dx.doi.org/10.5194/acp-20-7049-2020.

Sun, J., Hermann, M., Yuan, Y., Birmili, W., Collaud Coen, M., Weinhold, K., Madueño, L., Poulain, L., Tuch, T., Ries, L., Sohmer, R., Couret, C., Frank, G., Brem, B., Gysel, M., Ma, N., Wiedensohler, A., 2021. Long-term trends of black carbon and particle number concentration in the lower free troposphere in Central Europe. Environ. Sci. Europe 33, http://dx.doi.org/10.1186/s12302-021-00488-w.

Taheri, A., Aliasghari, P., Hosseini, V., 2019. Black carbon and PM2.5 monitoring campaign on the roadside and residential urban background sites in the city of Tehran. Atmos. Environ. 218, 116928. http://dx.doi.org/10.1016/j.atmosenv.2019.116928, URL: https://www.sciencedirect.com/science/article/pii/S1352231019305679.

Theil, H., 1950. A rank invariant method of linear and polynomial regression analysis, I, II, III. In: Proceedings of the Koninklijke Nederlandse Akademie Wetenschappen, Series a Mathematical Sciences, Vol. 53. 386–392, 521–525, 1397–1412.

Thomas, D.C., Christensen, J.H., Massling, A., Pernov, J.B., Skov, H., 2022. The effect of the 2020 COVID-19 lockdown on atmospheric black carbon levels in northeastern Greenland. Atmos. Environ. 269, 118853. http://dx.doi.org/10.1016/j.atmosenv.2021.118853, URL: https://www.sciencedirect.com/science/article/pii/S1352231021006750.

Uria-Tellaetxe, I., Carslaw, D.C., 2014. Conditional bivariate probability function for source identification. Environ. Model. Softw. 59, 1–9. http://dx.doi.org/10.1016/j.envsoft.2014.05.002.

Virkkula, A., Mäkelä, T., Hillamo, R., Yli-Tuomi, T., Hirsikko, A., Hämeri, K., Koponen, I.K., 2007. A simple procedure for correcting loading effects of aethalometer data. J. Air Waste Manage. Assoc. 57 (10), 1214–1222. http://dx.doi.org/10.3155/1047-3289.57.10.1214.

von Storch, H., 1999. Misuses of statistical analysis in climate research. In: von Storch, H., Navarra, A. (Eds.), Analysis of Climate Variability. Springer Berlin Heidelberg, Berlin, Heidelberg, pp. 11–26.

Wang, J., Nie, W., Cheng, Y., Shen, Y., Chi, X., Wang, J., Huang, X., Xie, Y., Sun, P., Xu, Z., Qi, X., Su, H., Ding, A., 2018. Light absorption of brown carbon in eastern China based on 3-year multi-wavelength aerosol optical property observations and an improved absorption ångström exponent segregation method. Atmos. Chem. Phys. 18 (12), 9061–9074. http://dx.doi.org/10.5194/acp-18-9061-2018, URL: https://acp.copernicus.org/articles/18/9061/2018/.

Weingartner, E., Saathoff, H., Schnaiter, M., Streit, N., Bitnar, B., Baltensperger, U., 2003. Absorption of light by soot particles: determination of the absorption coefficient by means of aethalometers. J. Aerosol Sci. 34 (10), 1445–1463. http://dx.doi.org/10.1016/S0021-8502(03)00359-8.

WHO, 2021. WHO Global Air Quality Guidelines. Particulate Matter ($PM_{2.5}$ and PM_{10}), Ozone, Nitrogen Dioxide, Sulfur Dioxide and Carbon Monoxide. World Health Organization, Geneva.

Yue, S., Pilon, P., Phinney, B., Cavadias, G., 2002. The influence of autocorrelation on the ability to detect trend in hydrological series. Hydrol. Process. 16 (9), 1807–1829. http://dx.doi.org/10.1002/hyp.1095.

Yus-Díez, J., Via, M., Alastuey, A., Karanasiou, A., Minguillón, M.C., Perez, N., Querol, X., Reche, C., Ivančič, M., Rigler, M., Pandolfi, M., 2022. Absorption enhancement of black carbon particles in a mediterranean city and countryside: effect of particulate matter chemistry, ageing and trend analysis. Atmos. Chem. Phys. 22 (13), 8439–8456. http://dx.doi.org/10.5194/acp-22-8439-2022, URL: https://acp.copernicus.org/articles/22/8439/2022/.

Zanatta, M., Gysel, M., Bukowiecki, N., Müller, T., Weingartner, E., Areskoug, H., Fiebig, M., Yttri, K., Mihalopoulos, N., Kouvarakis, G., Beddows, D., Harrison, R., Cavalli, F., Putaud, J., Spindler, G., Wiedensohler, A., Alastuey, A., Pandolfi, M., Sellegri, K., Swietlicki, E., Jaffrezo, J., Baltensperger, U., Laj, P., 2016. A European aerosol phenomenology-5: Climatology of black carbon optical properties at 9 regional background sites across europe. Atmos. Environ. 145, 346–364. http://dx.doi.org/10.1016/j.atmosenv.2016.09.035, URL: https://www.sciencedirect.com/science/article/pii/S135223101630735X.

Zhao, B., Jiang, J., Gu, Y., Diner, D., Worden, J., Liou, K.-N., Su, H., Xing, J., Garay, M., Huang, L., 2017. Decadal-scale trends in regional aerosol particle properties and their linkage to emission changes. Environ. Res. Lett. 12, http://dx.doi.org/10.1088/1748-9326/aa6cb2.

Zhao, W., Tan, W., Zhao, G., Shen, C., Yu, Y., Zhao, C., 2021. Determination of equivalent black carbon mass concentration from aerosol light absorption using variable mass absorption cross section. Atmos. Meas. Tech. 14 (2), 1319–1331. http://dx.doi.org/10.5194/amt-14-1319-2021, URL: https://amt.copernicus.org/articles/14/1319/2021/.

Zotter, P., Herich, H., Gysel, M., El-Haddad, I., Zhang, Y., Močnik, G., Hüglin, C., Baltensperger, U., Szidat, S., Prévôt, A.S.H., 2017. Evaluation of the absorption ångström exponents for traffic and wood burning in the Aethalometer-based source apportionment using radiocarbon measurements of ambient aerosol. Atmos. Chem. Phys. 17 (6), 4229–4249. http://dx.doi.org/10.5194/acp-17-4229-2017.